





ASMADO-based refined anti-disturbance low-speed control of PMSM

Huifan Wang^{1,2}  | Junze Tong^{1,2}  | Zhongshi Wang¹  | Dapeng Tian^{1,2} 

¹Key laboratory of Airborne Optical Imaging and Measurement, Changchun Institute of Optics, Fine Mechanics and Physics, Chinese Academy of Sciences, Changchun, China

²University of Chinese Academy of Sciences, Beijing, China

Correspondence

Zhongshi Wang, Key laboratory of Airborne Optical Imaging and Measurement, Changchun Institute of Optics, Fine Mechanics and Physics, Chinese Academy of Sciences, Changchun 130033, China.

Email: zhongshiwang@ciomp.ac.cn

Dapeng Tian, Key laboratory of Airborne Optical Imaging and Measurement, Changchun Institute of Optics, Fine Mechanics and Physics, Chinese Academy of Sciences, Changchun 130033, China.

Email: d.tian@ciomp.ac.cn

Funding information

National Natural Science Foundation of China, Grant/Award Numbers: T2122001, 62203421; National Key R&D Program of China, Grant/Award Number: 2022YFF1302000; Changchun Science and Technology Development Program, Grant/Award Number: 21SH03

Abstract

Permanent magnet synchronous motors (PMSMs) have expectant low-speed servo performance. However, complex nonlinear disturbances restrict the performance and lead to speed fluctuations, especially for small inertia PMSMs where the current-loop cannot be used in special operating conditions. This paper divides complex disturbances into periodic determinable disturbances and other indeterminate disturbances according to their characteristics. A refined anti-disturbance control (RADC) method is proposed to enable the inner loop to compensate for disturbances in targeted manners. Then ideal low-speed servo can be achieved using a simple outer loop controller. The proposed RADC consists of two parts. One is a backpropagation neural network based periodic disturbances compensator that is trained using the data from an iterative learning controller. The other is an adaptive sliding-mode-assisted disturbance observer that rapidly observes and compensates the residual disturbances. The convergence of the overall algorithm is analyzed. The effectiveness of the proposal is also verified by experiments.

1 | INTRODUCTION

Permanent magnet synchronous motor (PMSM) has the advantages of a simple structure, high power factor, high energy utilization, fast dynamic response and especially great low-speed performance. It has been widely used in high-precision machine tools, robotics, electric vehicles, and aerospace [1]. However, some PMSMs are complex controlled objects with multivariable, strong coupling, nonlinearity and variable parameters [2, 3]. Meanwhile, its defects such as cogging torque and shaft friction, as well as parameter uncertainties and environmental disturbances are inevitably introduced into the system. These multi-source disturbances seriously affect the low-speed control performance, especially for the condition of small inertia and load [4].

With the increasing requirements for control accuracy, reliability and real-time, the traditional control algorithm can no

longer meet the requirement. To improve the servo control performance, anti-disturbance is the core. Some nonlinear control theories have been proposed and developed, such as iterative learning controller (ILC) [5], neural network control [6], sliding mode control (SMC) [7] etc. These control methods have been used in PMSM speed control systems.

ILC has the mechanism of memory storage and feedback correction. This algorithm only needs the error value of the past time, and it does not need the specific parameters of the system. The core idea of ILC is to use the last output of the controller and the current error to correct the current output of the controller to achieve the purpose of suppressing periodic disturbances. It is described as a “modeless” or “data-driven” control method [8, 9]. Compared with traditional controllers, the ILC has strong adaptability and repeatability, and the optimal control quantity can be obtained through the learning law. An improved ILC was proposed in ref. [10]. Compared

This is an open access article under the terms of the [Creative Commons Attribution-NonCommercial-NoDerivs](https://creativecommons.org/licenses/by-nc-nd/4.0/) License, which permits use and distribution in any medium, provided the original work is properly cited, the use is non-commercial and no modifications or adaptations are made.

© 2023 The Authors. *IET Power Electronics* published by John Wiley & Sons Ltd on behalf of The Institution of Engineering and Technology.

with conventional ILC, this method combined with a classical PID speed controller further suppressed the speed fluctuation caused by torque ripple through Fourier series expansion in the frequency domain.

However, ILC takes several iterations to achieve disturbance suppression, which needs a longer time. Secondly, ILC only has an obvious inhibition effect on periodic disturbances. ILC is sensitive to the uncertainty of system parameters, which makes it have a weak anti-disturbance capability. There are various uncertain and abrupt disturbances in the actual working condition, and these disturbances will also be introduced into the control quantity through the learning law [11].

The neural network realizes the mapping function from input to output, and it is also successfully used in the PMSM control [12]. Some neural networks have simple structures, strong plasticity, clear mathematical meaning, and clear learning steps, and have very good advantages in function approximation, pattern recognition etc. A neural network can realize complex nonlinear mapping. By training the neural network with a large amount of data, the network structure and neuron parameters can be obtained, which is particularly suitable for solving problems with complex internal mechanisms. However, solely relying on a neural network is still unable to cope with complex and time-varying disturbances for PMSM servo control.

To improve the anti-disturbance, SMC is a feasible solution that has strong robustness [13]. It shows good control performance in nonlinear systems and has become a research hotspot. In ref. [14], SMC has been successfully applied to PMSM and achieved a good control effect. However, the discontinuous switching characteristics of SMC make it inevitable to have chattering which not only affects the accuracy of the system but also accelerates energy consumption. To reduce the chattering of the sliding mode controller, scholars have proposed various improved schemes. A new approach law was designed in ref. [15]. A fuzzy control method was introduced to adjust the gain of SMC in real-time in ref. [16]. Besides, an adaptive sliding mode controller (ASMC) was designed to estimate the switching gain using an adaptive law to reduce system chattering caused by a fixed switching gain in ref. [17].

These anti-disturbance methods are feasible for any disturbances. However, it also means great conservatism in the design of the control algorithm. The desired low-speed tracking of the PMSM cannot be achieved by simply using one of the ILC, SMC, or BPNN algorithms or a simple superposition of them. In fact, the actual PMSM servo control system can be described as a mathematical model with multi-source disturbance. Some disturbances have their own patterns of changing. Considering these characteristics is quite helpful to decrease the conservatism.

The composite hierarchical anti-disturbance control (CHADC) theory was proposed for multi-source disturbance rejection based on disturbance classification modelling and expanded the idea of combining disturbance observer (DOB) with other anti-disturbance control methods to deal with multiple disturbances [18, 19]. Its main purpose is to

analyze the characteristics of various disturbances, make full use of the characteristics to carry out classification modelling and adopt different methods to achieve better disturbance compensation.

The idea of CHADC can be separated into two layers. The inner layer includes a DOB and an additional disturbance compensator, and the outer layer includes a disturbance rejection controller. This hierarchical structure not only simplifies the design and analysis but also improves the control accuracy of the system. The above CHADC is now regarded as a refined anti-disturbance control (RADC) method that is customized [20]. However, CHADC still has its shortcoming. The use of DOB in the low-frequency domain can well realize the compensation of equivalent interference and improve the performance of the motor system. However, it cannot compensate for the high-frequency components of the disturbance such as sudden external force and coulomb friction of the motor [21]. A sliding mode assisted disturbance observer (SMADO) was proposed by skillfully combining SMC with DOB [22]. It uses the sliding mode technique to assist the DOB to estimate and compensate for the wide-bandwidth disturbances. Then, a new control method is expected by systematically combining both the ideas of RADC and SMADO.

To improve the low-speed servo performance of the PMSM when the current-loop-free control method is used, this paper considers the various complex disturbances as periodic determinable disturbances and other indeterminate residual disturbances. A new method of RADC is proposed. When this method is added to the system as an internal loop control, the system can illustrate an expected highly linear characteristic even though there are complex various disturbances. The convergence is proved. Besides, the effectiveness of the proposal is also verified by objective experiments. The main contributions of this paper are as follows:

- (i) A BPNN-based offline disturbance compensator is designed to realize a refined, accurate and fast disturbance rejection by training with the data from an ILC. The effect of periodic determinable disturbances on the system is reflected in the output of an ILC. Therefore, an ILC is designed to obtain optimal training datasets rather than being used as the final controller. These datasets are used to train the BPNN to fit a function between the periodic disturbance and position response of the PMSM.
- (ii) To further compensate for the residual indeterminate disturbances, an ASMADO with BPNN-based refined compensator is designed. The rapid switching action provides the ability to deal with the high-frequency component of the residual disturbance that DOB cannot observe. This method eliminates the difference between the expected dynamics and the actual dynamics of the PMSM. Moreover, a piecewise adaptive switching gain is designed. When the state of the system deviates from the preset boundary, a large and fixed switching gain is given immediately. If the state of the system is within the boundary, the switching gain is determined by the adaptive law and gradually attenuates to zero, thus reducing the chattering.

The main contents of the following sections are given below. Section 2 gives the mathematical model of the PMSM. Section 3 presents the design of the RADC. In Section 4, the convergence of the RADC is analyzed using Lyapunov functions. Section 5 shows the experimental results. Finally, Section 6 concludes the whole paper.

2 | PROBLEM FORMULATIONS

2.1 | System modelling

In order to analyze the speed control system of PMSM, the mathematical model is established.

The mechanical motion equation of PMSM is:

$$\frac{d\omega_m(t)}{dt} = \frac{1}{J}[T_e(t) - B\omega_m(t) - T_L(t)], \quad (1)$$

where, ω_m denotes the mechanical speed, T_L is the load torque, T_e is the electromagnetic torque, J and B represent the equivalent moment of inertia and equivalent damping coefficient, respectively.

In this paper, $i_d = 0$ control strategy is adopted, and i_d is the d -axis component of stator current. Then the electromagnetic torque equation is:

$$T_e(t) = \frac{3}{2}p\psi_f i_q(t) = K_t i_q(t), \quad (2)$$

where, p represents the number of pole pairs, ψ_f denotes the permanent magnet flux linkage, K_t is the motor torque coefficient, and i_q is the q -axis component of stator current.

Considering the actual PMSM, it is difficult to satisfy the strict symmetry, i.e. the three-phase windings and equivalent inductances are not identical. The presence of this asymmetry leads to a more complex coupling of the current equations in the d - q axes after a mathematical transformation.

$$\begin{bmatrix} u_d \\ u_q \end{bmatrix} = \begin{bmatrix} R_s + \Delta R_{d1} & \Delta R_{q2} \\ \Delta R_{d2} & R_s + \Delta R_{q1} \end{bmatrix} \begin{bmatrix} i_d \\ i_q \end{bmatrix} + \begin{bmatrix} L_{d1} + \Delta L_{d1} & \Delta L_{q2} \\ \Delta L_{d2} & L_{q1} + \Delta L_{q1} \end{bmatrix} \begin{bmatrix} \frac{di_d}{dt} - \omega_e i_q \\ \frac{di_q}{dt} + \omega_e i_d \end{bmatrix} + \omega_e \begin{bmatrix} \psi_d \\ \psi_q \end{bmatrix}. \quad (3)$$

where u_d and u_q are the d - q axes components of the stator voltage, respectively, L_{d1} and L_{q1} are the d - q axes equivalent inductances, respectively, R_s is the stator resistance, ω_e is the electrical angular velocity. ψ_d and ψ_q are the d and q axes components of the stator magnetic flux linkage, respectively. And ΔR_j , as well as, ΔL_j represent the parameter uncertainties caused by asymmetry, respectively.

When magnetic field orientation control is used in an ideal permanent magnet synchronous motor, the q -axis magnetic flux

linkage ψ_q is equal to the permanent magnet flux linkage ψ_f and contains only the DC component, i.e.

$$\begin{bmatrix} \psi_d \\ \psi_q \end{bmatrix} = \begin{bmatrix} 0 \\ \psi_f \end{bmatrix}. \quad (4)$$

However, due to core saturation and permanent magnet manufacturing errors, it is difficult to achieve an ideal sinusoidal flux density distribution for the flux harmonics. Combining Equations (3) and (2), flux harmonics cause distortions in the current, which cause electromagnetic torque pulsation. And Equation (1) shows that torque pulsation causes speed pulsation. At this point, the magnetic flux linkage generated by the three-phase current is represented in the d - q coordinate system as [10]:

$$\begin{bmatrix} \psi_d(\theta_e) \\ \psi_q(\theta_e) \end{bmatrix} = \begin{bmatrix} \psi_{d0} + \sum_{i=1}^{\infty} \psi_{di} \cos(6i\theta_e) \\ \psi_{q0} + \sum_{i=1}^{\infty} \psi_{qi} \cos(6i\theta_e) \end{bmatrix}, \quad (5)$$

where ψ_{d0} and ψ_{q0} are the DC components of the stator magnetic flux linkage in the d axis and q axis respectively, ψ_{di} and ψ_{qi} are the amplitudes of the i th harmonic flux linkage, and θ_e is the electrical angle.

At the same time, cogging torque in the PMSM can also cause periodic fluctuations in the electromagnetic torque, which can cause speed fluctuations in the steady state and affect the control accuracy of the motor. The torque pulsation due to the cogging effect is a periodic function of the rotor position and can be expressed in the Fourier series as [23]:

$$T_{\text{cog}}(\theta) = \sum_{j=1}^{\infty} T_j \sin(mj\theta), \quad (6)$$

where $\theta = \theta_e/p$ is the mechanical angular position, T_j is the Fourier coefficient and m is the least common multiple of the number of stator slots and the number of poles.

Since the rotational inertia and damping coefficients of the motor are not constant coefficients, and the parameters usually obtained by system identification are constants, Equation (1) can be expressed as:

$$(J_n + \Delta J) \frac{d\omega_m(t)}{dt} + (B_n + \Delta B)\omega_m(t) = T_e(t) - T_L(t), \quad (7)$$

where J_n and B_n are the equivalent nominal rotational inertia and equivalent nominal damping coefficients, respectively, obtained by identifying the system, and ΔJ and ΔB denote the uncertainty part of the parameters, respectively.

In addition, the use of control with the current-loop in special cases can bring disadvantages to the servo system, such as parameter mismatch in the current loop, current measurement

errors, power device tube voltage drop, air-gap magnetic field distortion, and dead time of the inverter can lead to a large number of harmonic components in the stator current, and these current harmonics can lead to periodic oscillations in the steady state of the speed, thus reducing the operational performance of the servo control system [24]. However, the simple removal of the current loop and the use of only a speed-loop control leads to problems such as low control stiffness and large torque fluctuations. This paper, therefore, uses a current-loop-free control method based on space vector pulse width modulation (SVPWM) for velocity closed-loop control research.

In summary, the lumped disturbance $d(t)$ includes d - q inter-axes current coupling, parameter uncertainty, flux harmonics, cogging torque, shaft friction, and other non-determinable non-linear disturbances. In this paper, the above disturbances are briefly classified according to their characteristics and the lumped disturbance $d(t)$ is divided into two categories: periodic disturbances $d_p(t)$ and other non-periodic disturbances $d_{\text{other}}(t)$.

$$d(t) = d_p(t) + d_{\text{other}}(t). \quad (8)$$

Besides, to make the control program generic (i.e. the program can still be directly ported and used if the inverter is powered by a different DC bus voltage.), the control program in this paper makes use of the normalisation method, using a 16 bit signed fixed-point number as the control input, then the mechanical equations of motion of the motor can be transformed into:

$$J_n \frac{d\omega_m(t)}{dt} + B_n \omega_m(t) = u(t) + d(t), \quad (9)$$

where $u(t)$ denotes the equivalent control input.

2.2 | Control objectives

The control objective of this paper is to use the RADC method to improve the immunity of a specific controlled object to disturbances and to reduce velocity fluctuations in the absence of current-loop control. For the periodic determinable disturbance $d_p(t)$ and the other non-periodic indeterminate disturbance $d_{\text{other}}(t)$, their equivalent disturbances are obtained using function fitting and observation, respectively, and targeted compensation is performed in the control inner loop.

$$J_n \frac{d\omega_m(t)}{dt} + B_n \omega_m(t) = u(t) + d(t) - \hat{d}_p(t) - \hat{d}_{\text{other}}(t). \quad (10)$$

3 | REFINED ANTI-DISTURBANCE CONTROL OF PMSM

For the complex disturbances of PMSM, we develop the RADC method to compensate for and suppress the disturbances. The

overall control algorithm contains a compensator for periodic disturbances and a compensator for residual disturbances. These two parts constitute the refined anti-disturbance internal loop control. In practice, an additional outer-loop controller, such as a PID controller, is easy to design. In the following representation, we will omit the argument t . And bold fonts represent vectors.

3.1 | Compensation for periodic disturbances

BPNN adopts supervised learning. Therefore, when using BPNN to fit the nonlinear relationship between the angular position and the periodic determinable disturbance of PMSM, it is required that mechanical angular position θ is the input dataset and the disturbance d_p is the output dataset. Moreover, the datasets need to reflect the relationship to be fitted as fully as possible, so that the generalization ability of BPNN can be used to make correct predictions for the data that is not in the training samples. Therefore, an ILC for PMSM based on the space domain is designed with the help of the ILC's ability to restrain periodic disturbances, to obtain more comprehensive input and output datasets of BPNN. The block diagram of ILC is shown in Figure 1, where k is the iterations ($k = 1, 2, 3, \dots$), e_k is the velocity error, Memory¹ and Memory² represent arrays used to store control quantity. Select the corresponding array to store or read the control quantity according to the value of k .

As we know, the larger the capacity of the array, the more data can be stored, and the better the learning effect. But the stored data will occupy a lot of resources of the chip. In this paper, the control quantity at the integer angle and half angle is stored when the motor rotates at a low and constant speed. Each revolution of the motor is an iteration cycle. The motion of any position of the motor in this iterative learning process is compensated by linear interpolation through the control quantity stored in the last iteration cycle, to achieve the effect of restraining the periodic disturbances.

Store the control quantity:

$$\left\{ \begin{array}{l} \text{Memory}[0] = u_{k-1}(0) \\ \text{Memory}[1] = u_{k-1}(0.5) \\ \vdots \\ \text{Memory}[n] = u_{k-1}\left(\frac{n}{2}\right) \\ \vdots \\ \text{Memory}[719] = u_{k-1}(359.5) \end{array} \right., \quad n = 0, 1, 2, \dots, 719, \quad (11)$$

where $u_{k-1}\left(\frac{n}{2}\right)$ represents the control quantity of ILC output at position $\theta = \frac{n}{2}$ at iteration $k - 1$.

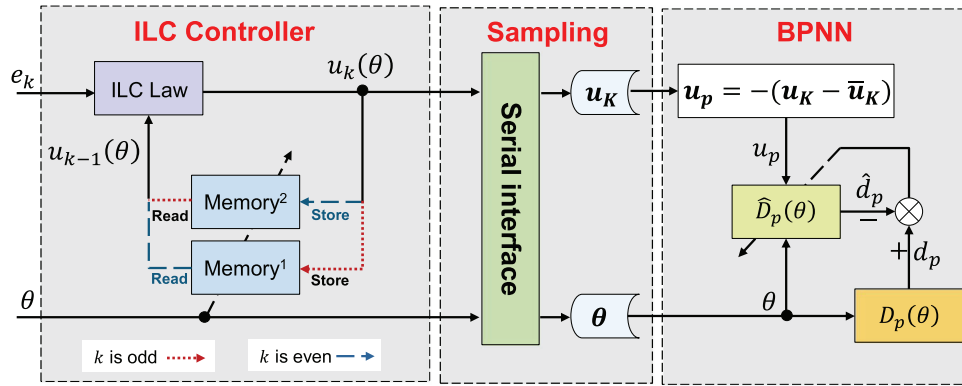


FIGURE 1 Block diagram of ILC, data sampling, and BPNN training.

Read the control quantity stored in the last iteration:

$$u_{k-1}(\theta) = 2(\text{Memory}[\lfloor 2\theta \rfloor + 1] - \text{Memory}[\lfloor 2\theta \rfloor]) \times \left(\theta - \frac{\lfloor 2\theta \rfloor}{2} \right) + \text{Memory}[\lfloor 2\theta \rfloor], \quad \theta \in [0, 360^\circ), \quad (12)$$

where $\lfloor * \rfloor$ represents rounding down function.

The ILC Law is

$$\begin{cases} e_k(\theta) = \omega_d(\theta) - \omega_k(\theta), \\ u_k(\theta) = u_{k-1}(\theta) + P e_k(\theta) + I \int e_k(\theta) dt, \end{cases} \quad (13)$$

where ω_k is the mechanical angular velocity of the motor in the process of iteration k , ωd is the speed command, P and I represent the proportional and integral learning gain of ILC respectively.

Remark 1. The ILC used in the paper is not directly applied to the final RADC controller. And ILC, as a well-established application in the field of control, has proven its stability in several papers. I add an analysis of the stability of the ILC in the form of a remark.

$L(s)$ is the learning law function, and $G(s)$ is the controlled object.

$$L(s) = \frac{Ps + I}{s}, \quad (14)$$

$$G(s) = \frac{1}{Js + B}, \quad (15)$$

that

$$\omega(s) = \frac{(Ps + I)\omega d(s) + s u_{k-1}(s)}{Js^2 + Bs + Ps + I}, \quad (16)$$

where $J > 0, B > 0, P > 0, I > 0$, so in the same iteration, the system is stable according to Routh stability criterion.

$$\begin{cases} u_k(s) = u_{k-1}(s) + L(s)e_k(s), \\ e_{k-1}(s) = \omega d(s) - \omega_{k-1}(s), \\ \omega_{k-1}(s) = G(s)u_{k-1}(s), \\ \omega_k(s) = G(s)u_k(s). \end{cases} \quad (17)$$

Combining Equation (17), the transfer function of error changes with the number of iterations can be expressed as:

$$e_k(s) = \omega d(s) - \omega_k(s) = \frac{1}{1 + G(s)L(s)} e_{k-1}(s). \quad (18)$$

Convergence analysis of ILC from the perspective of the frequency domain.

$$\| \frac{e_k(j\omega)}{e_{k-1}(j\omega)} \|_\infty = \| \frac{1}{1 + G(j\omega)L(j\omega)} \|_\infty \leq r \leq 1. \quad (19)$$

Equation (19) is the convergence condition of ILC. In the satisfied frequency band, $e_0(j\omega)$ exists at the beginning of the first iteration. When $k \rightarrow \infty$, the error approaches 0, that is,

$$\begin{aligned} \| e_k(j\omega) \|_\infty &= \| \frac{1}{1 + G(j\omega)L(j\omega)} \|_\infty^k \| e_0(j\omega) \|_\infty \\ &\leq r^k \| e_0(j\omega) \|_\infty \rightarrow 0. \end{aligned} \quad (20)$$

The more iterations, the better the control accuracy. With the increase of iterations, when the change of control effect is not obvious in the K th iteration, according to the principle of equivalence, the angular position of the motor and the control quantity u_k are sampled by the serial interface at a sampling frequency f .

When the speed command ωd is constant, the periodic determinable disturbance can be considered as a higher-order angular position function. The DC component of the control quantity that is used to keep the motor rotating at a constant speed is

TABLE 1 Functions and algorithms setting of BPNN.

Functions and algorithms	Values
Transfer function of hidden layers	Tansig
Transfer function of output layer	Purelin
Training algorithm	Trainlm (Levenberg–Marquardt)
Performance algorithm	MSE (mean squared error)

removed and the AC component is extracted.

$$\begin{cases} u_{AC,K}(\theta) = u_K(\theta) - \bar{u}_K, \\ u_p(\theta) = -u_{AC,K}(\theta). \end{cases} \quad (21)$$

As shown in Equation (21), \bar{u}_K represents the mean value of the data set of $u_K(\theta)$, and $u_p(\theta)$ is the value of the periodic determinable disturbance d_p equivalent to the control quantity when the angular position is θ , which is bounded.

As shown in Figure 1. Let u_p replace d_p as the output dataset of training BPNN. By learning the input and output datasets, BPNN uses the error backpropagation algorithm to minimize the mean square error of the network and to identify the functional relationship $D_p(\theta)$ between the input and output of the system. And $\hat{D}_p(\theta)$ is the fitting result of BPNN. Table 1 lists the functions and algorithms used in BPNN training.

The number of nodes in the input layer and output layer of the network is determined according to the actual problem. The number of hidden layers and their nodes have a great impact on the performance of BPNN. Generally, too few hidden layers and hidden layer nodes will make the network unable to learn. More hidden layers and nodes may bring better performance and reduce error to a certain extent. However, it will undoubtedly lead to a long calculation time. The network may also be overfitting. It is worth noting that there is no ideal method to determine the number of layers and nodes of the hidden layer [25]. And it is mostly determined by the experience of the designer and a large number of training results. As shown in Figure 2, taking the BPNN with three hidden layers, a single input and a single output as an example, the identification result can be expressed as:

$$\begin{cases} o^1 = f^1(w^1\theta + b^1), \\ o^2 = f^1(w^2o^1 + b^2), \\ o^3 = f^1(w^3o^2 + b^3), \\ \hat{d}_p = f^2(w^4o^3 + b^4), \end{cases} \quad (22)$$

where w represents the weight parameter, b represents the offset parameter, o is the output of each node, $f^1(*)$ and $f^2(*)$ are transfer functions of hidden layer nodes and output layer nodes, respectively.

When the neural network converges, the periodic determinable disturbance function identified by BPNN is approximate to the actual disturbance function, and the disturbance

compensation value also approximates the real disturbance, i.e.

$$\hat{d}_p \rightarrow d_p. \quad (23)$$

3.2 | Compensation for residual disturbances

To further improve the control performance of the PMSM low-speed servo system, ASMADO is designed. The ASMC method is used to assist DOB to estimate and compensate for the high-frequency disturbance that cannot be compensated. At the same time, the adaptive law is used to estimate the switching gain of the SMC. The block diagram is shown in Figure 3.

$$\begin{cases} \dot{\xi} = -g\xi - g(-Bn\omega m + un + gJn\omega m), \\ \hat{d}_{DOB} = \xi + gJn\omega m, \end{cases} \quad (24)$$

where, \hat{d}_{DOB} is the observation value of DOB, g is the cut-off angle frequency of DOB, ξ is the state variable of DOB.

The periodic determinable disturbance d_p and its compensation \hat{d}_p are bounded. According to Equation (23), we define \tilde{d}_p as the part of periodic determinable disturbance that is not compensated by \hat{d}_p , and it is bounded. So

$$\tilde{d}_p = d_p - \hat{d}_p. \quad (25)$$

Next we define d_{res} is the residual disturbance,

$$d_{res} = d_{other} + \tilde{d}_p. \quad (26)$$

And there is an estimation error \tilde{d}_{res} between d_{res} and \hat{d}_{DOB} , i.e.:

$$\tilde{d}_{res} = d_{res} - \hat{d}_{DOB}. \quad (27)$$

The nominal dynamic model can be described as follows:

$$Jn\dot{\omega}_n + Bn\omega_n = un + \hat{d}_{DOB} + \hat{d}_{ASMC}. \quad (28)$$

where, \hat{d}_{ASMC} is the compensation amount of ASMC for \tilde{d}_{res} . The observed value of ASMADO is

$$\hat{d}_{res} = \hat{d}_{DOB} + \hat{d}_{ASMC}, \quad (29)$$

To design \hat{d}_{ASMC} , nominal error en is defined as follows:

$$en = \omega m - \omega_n. \quad (30)$$

Design sliding mode surface:

$$s = en + c \int endt, \quad (c > 0), \quad (31)$$

$$\dot{s} = \frac{\tilde{d}_{res} - \hat{d}_{ASMC} - Bnen}{Jn} + cen. \quad (32)$$

By $\dot{s} = 0$ and $\tilde{d}_{res} = 0$ gets equivalent \hat{d}_{ASMC_1} :

$$\hat{d}_{ASMC_1} = Jncen - Bnen. \quad (33)$$

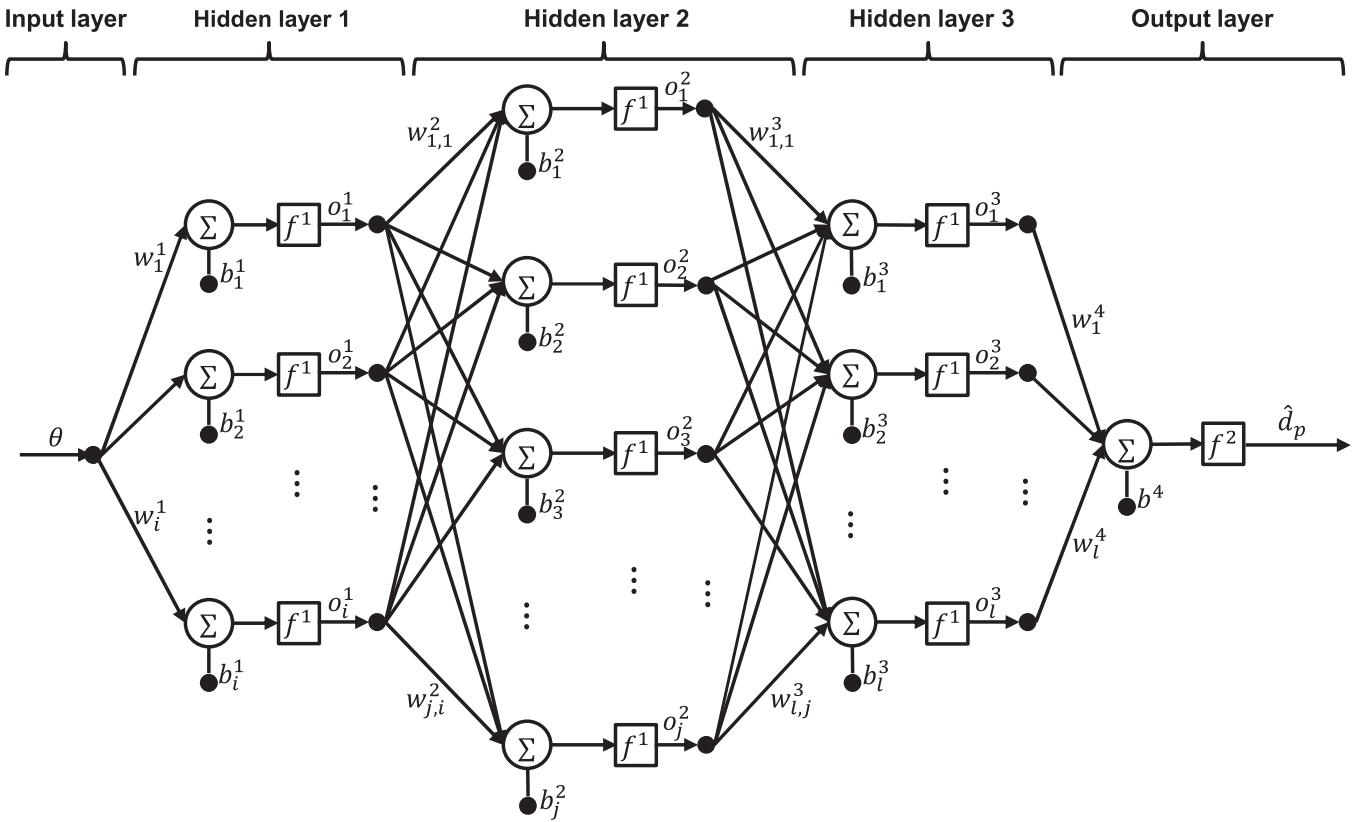


FIGURE 2 Identification result of BPNN.

The switching term is designed as follows:

$$\hat{d}_{ASMC_2} = \lambda \text{sgn}(s) + \beta s, \quad (\beta > 0), \quad (34)$$

where $\text{sgn}(\ast)$ is a symbolic function.

$$\text{sgn}(s) = \begin{cases} 1, & s > 0, \\ 0, & s = 0, \\ -1, & s < 0. \end{cases} \quad (35)$$

To adjust the switching gain of \hat{d}_{ASMC_2} to weaken the difference between the expected and actual dynamics caused by error \tilde{d}_{res} , the switching gain is designed as follows:

$$\lambda = \begin{cases} \hat{\eta}, & |s| < \nu, \\ \Lambda, & |s| \geq \nu, \end{cases} \quad (36)$$

here, $\Lambda \in \mathbb{R}^+$ is a constant, $\Lambda > \eta$, and parameter $\nu \in \mathbb{R}^+$ is a threshold, which determines the thickness of the sliding mode boundary layer. η is the upper bound of \tilde{d}_{res} , which is unknown. When $|s| < \nu$, the estimated value $\hat{\eta}$ of η is used as the switching gain of ASMC. The adaptive algorithm is used to estimate η , and the adaptive law is as follows:

$$\dot{\hat{\eta}} = \frac{\sigma_1}{J_n} |s| - \frac{\sigma_2}{J_n} \hat{\eta}, \quad (\sigma_1, \sigma_2 > 0). \quad (37)$$

According to the design principle of ASMC, the compensation value is

$$\hat{d}_{ASMC} = \hat{d}_{ASMC_1} + \hat{d}_{ASMC_2}. \quad (38)$$

According to the theory of ASMADO, the observation error of ASMADO can be expressed as:

$$\Delta = \hat{d}_{ASMC} - \tilde{d}_{res} \rightarrow 0. \quad (39)$$

In other words,

$$\hat{d}_{res} \rightarrow d_{res}. \quad (40)$$

By using the proposal, the overall control block diagram is illustrated in Figure 3. The internal loop is the proposed RADC that compensates for both the periodic determinable disturbance and indeterminate residual disturbance. The outer loop uses a normal PI controller to realize a speed servo. The flow of the RADC implementation is shown in Figure 4.

4 | STABILITY PROOF OF THE PROPOSED REFINED ANTI-DISTURBANCE CONTROL METHOD

In order to prove the stability of RADC, an assumption and three lemmas are given:

Lemma 3. For $\mathcal{A} = [\alpha_1, \alpha_2, \dots, \alpha_n]^T \in \mathbb{R}^n$, the following inequality holds:

$$(\alpha_1^2 + \alpha_2^2 + \dots + \alpha_n^2)^{\frac{1}{2}} \leq (|\alpha_1| + |\alpha_2| + \dots + |\alpha_n|). \quad (46)$$

To prove the stability of RADC, we give the following theorem.

Theorem 1. Based on the condition given in Assumption 1, the proposed RADC is stable, and \tilde{d}_{res} , s , and e_n are ultimately uniformly bounded and will also converge to the neighbourhood of zero in finite-time.

Proof. The process of proving the stability of the RADC is divided into the following three steps. \square

The periodic disturbance d_p is bounded. From Equation (22) it follows that the compensation value \hat{d}_p of periodic disturbance is also bounded. Combining Equations (23) and (25) that the norm of \hat{d}_p is bounded, i.e.

$$\|\hat{d}_p\| = \gamma. \quad (47)$$

Step 1: It is proved that the error \tilde{d}_{res} converges to a bounded set in the domain $\tilde{d}_{res} = 0$. The following Lyapunov functions are constructed:

$$V_3 = \frac{1}{2}\tilde{d}_{res}^2. \quad (48)$$

Combined Equations (24) and (27), taking the time derivative of V_3 .

$$\begin{aligned} \dot{V}_3 &= \tilde{d}_{res}\dot{\tilde{d}}_{res} \\ &= \tilde{d}_{res}(\dot{d}_{res} - \dot{\hat{d}}_{DOB}) \\ &= \tilde{d}_{res}[\dot{d}_{res} - (\dot{\xi} + gJn\dot{\omega})] \\ &= \tilde{d}_{res}[\dot{d}_{res} - \tilde{g}_{res}] \\ &= \tilde{d}_{res}\dot{d}_{res} - \tilde{g}_{res}^2. \end{aligned} \quad (49)$$

Although the time derivative of d_{res} is unknown, it is assumed to be bounded, which means that there is a positive constant ϕ meet $|\dot{d}_{res}| \leq \phi$, therefore,

$$\dot{V}_3 \leq \phi|\tilde{d}_{res}| - \tilde{g}_{res}^2 = -|\tilde{d}_{res}|(g|\tilde{d}_{res}| - \phi). \quad (50)$$

If $|\tilde{d}_{res}| \geq \frac{\phi + \tau_3}{g}$, and $\tau_3 > 0$, then,

$$\dot{V}_3 \leq -\tau_3|\tilde{d}_{res}| = -\sqrt{2}\tau_3V_3^{\frac{1}{2}}. \quad (51)$$

According to Lemma 1, Equation (51) satisfies the convergence criterion. The error $|\tilde{d}_{res}|$ con-

verges to the neighbourhood of $\tilde{d}_{res} = 0$ at time $t_3 = \sqrt{2}V_3^{\frac{1}{2}}(0)/(\tau_3)$.

Step 2: After time t_3 , to prove the stability of the proposed ASMADO, construct another Lyapunov function as follows:

$$V_4 = \frac{\tilde{d}_{res}^2}{2} + \frac{s^2}{2} + \frac{\tilde{\eta}^2}{2\sigma_1}. \quad (52)$$

Where, $\tilde{\eta} = \eta - \hat{\eta}$, and $\eta \geq |\tilde{d}_{res}| + m$ with $m > 0$. The time derivative of V_4 is

$$\begin{aligned} \dot{V}_4 &= \tilde{d}_{res}\dot{\tilde{d}}_{res} + s\dot{s} - \frac{\tilde{\eta}\dot{\tilde{\eta}}}{\sigma_1} \\ &= \tilde{d}_{res}(\dot{d}_{res} - \tilde{g}_{res}) + s(\dot{e}_n + c\dot{e}_n) - \tilde{\eta}\left(\frac{|s|}{J_n} - \frac{\sigma_2}{J_n\sigma_1}\tilde{\eta}\right) \\ &= \tilde{d}_{res}(\dot{d}_{res} - \tilde{g}_{res}) + \frac{s}{J_n}\tilde{d}_{res} - \eta\text{sgn}(s) + \hat{\eta}\text{sgn}(s) \\ &\quad - \lambda\text{sgn}(s) - \beta|s| + \frac{\sigma_2}{J_n\sigma_1}\tilde{\eta}\hat{\eta} \\ &\leq \tilde{d}_{res}(\dot{d}_{res} - \tilde{g}_{res}) + \frac{s}{J_n}[\tilde{d}_{res} - \eta\text{sgn}(s) - \beta|s|] + \frac{\sigma_2}{J_n\sigma_1}\tilde{\eta}\hat{\eta} \\ &\leq \tilde{d}_{res}(\dot{d}_{res} - \tilde{g}_{res}) - \frac{|s|}{J_n}[\eta - |\tilde{d}_{res}|] - \frac{\beta|s|^2}{J_n} + \frac{\sigma_2}{J_n\sigma_1}\tilde{\eta}\hat{\eta}. \end{aligned} \quad (53)$$

The following inequality holds:

$$\tilde{\eta}\hat{\eta} = \tilde{\eta}(\eta - \tilde{\eta}) \leq \frac{\eta^2 - \tilde{\eta}^2}{2}. \quad (54)$$

When the time reaches t_3 , according to Equation (54), Equation (53) can be written as:

$$\begin{aligned} \dot{V}_4 &\leq -\tau_3|\tilde{d}_{res}| - \frac{m}{J_n}|s| + \frac{\sigma_2}{J_n\sigma_1}\tilde{\eta}\hat{\eta} \\ &\leq -\tau_3|\tilde{d}_{res}| - \frac{m}{J_n}|s| - \frac{\sigma_2|\tilde{\eta}|}{2J_n\sigma_1} + \frac{\sigma_2(|\tilde{\eta}| + \eta^2 - \tilde{\eta}^2)}{2J_n\sigma_1}. \end{aligned} \quad (55)$$

Where, formula $\frac{\sigma_2(|\tilde{\eta}| + \eta^2 - \tilde{\eta}^2)}{2J_n\sigma_1}$ has upper bound $\varrho = \frac{\sigma_2(1+4\eta^2)}{8J_n\sigma_1}$. According to Lemma 3, Equation (55) can be written as:

$$\begin{aligned} \dot{V}_4 &\leq \min\left\{\sqrt{2}\tau_3, \frac{\sqrt{2}m}{J_n}, \frac{\sigma_2}{J_n\sqrt{2\sigma_1}}\right\}\left(\frac{|\tilde{d}_{res}|}{\sqrt{2}} + \frac{|s|}{\sqrt{2}} + \frac{|\tilde{\eta}|}{\sqrt{2\sigma_1}}\right) + \varrho \\ &\leq -\tau_4V_4^{\frac{1}{2}} + \varrho. \end{aligned} \quad (56)$$

Where, $\tau_4 = \min\{\sqrt{2}\tau_3, \sqrt{2}m/J_n, \sigma_2/(J_n\sqrt{2\sigma_1})\}$.

According to Lemma 2, in time $t_4 = t_3 + 2V_4^{\frac{1}{2}}(t_3)/(\tau_4\mu)$ with $0 < \mu < 1$, the sliding mode surface s and the error $\tilde{\eta}$ can converge to the neighbourhood of 0.

Step 3: After time t_4 , we will prove that the error e_n can reach the bounded set containing the equilibrium point $e_n =$

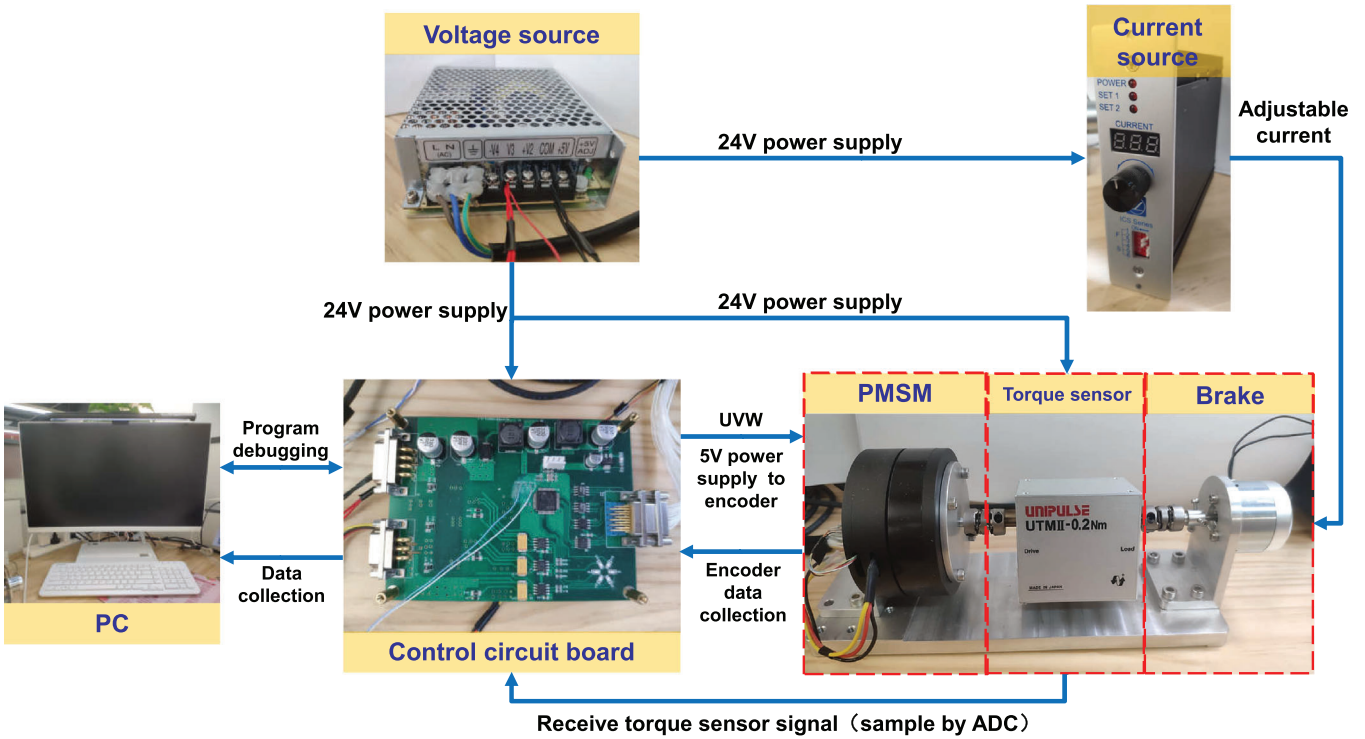


FIGURE 5 Experimental platform.

0, and select the following Lyapunov function:

$$V_5 = \frac{1}{2}en^2. \quad (57)$$

The time derivative of V_5 is

$$\begin{aligned} \dot{V}_5 &= en\dot{e}n = en(\dot{s} - cen) \\ &\leq en\dot{s} - cen^2 \leq |en||\dot{s}| - cen^2 \\ &= -(c|en| - |\dot{s}|)|en|. \end{aligned} \quad (58)$$

If $|en| \geq (|\dot{s}| + \tau_5)/c$ with $\tau_5 > 0$, Equation (58) can be written as

$$\dot{V}_5 \leq -\tau_5|en| = -\sqrt{2\tau_5}V_5^{\frac{1}{2}}. \quad (59)$$

According to Lemma 1, Equation (59) satisfies the convergence criterion. The error en converges to the neighbourhood of $en = 0$ at time $t_5 = t_4 + \sqrt{2}V_5^{\frac{1}{2}}(t_4)/(\tau_5)$.

To sum up, the proof of Theorem 1 is complete.

5 | EXPERIMENTS

In this section, an experimental platform is built as shown in Figure 5. The experimental platform is mainly composed of the personal computer, control circuit board, PMSM, the mag-

netic encoder (IC-MU MAGNETIC OFF-AXIS POSITION ENCODER), torque sensor (UTM-0.2Nm), hysteresis brake (HB-201B), voltage source, and current source (ICS-500).

The voltage source provides 24 V to the control board, torque sensor, and current source. The current source provides a stable and adjustable current for the hysteresis brake. The computer is used for program debugging with the control board and for collecting useful data via the serial interface. The control circuit board takes STM32F405RGT6 as the core chip. In addition, the control circuit board has the following main functions: provide a three-phase drive signal for the PMSM, receive torque sensor signal through analogue-to-digital converter (ADC), supply 5 V voltage to the magnetic encoder in the motor, receive the position information output by the encoder and calculate the control quantity through the control algorithm. In this experiment, a PMSM with 14 polar pairs is selected. The encoder is a 20 bit encoder. The measuring range of the torque sensor is 0 to 0.2 N m, and the resolution is 0.01 mN m. The rated torque of the hysteresis brake is 0.2 N m.

To verify the superiority of the proposed methods, the following two comparison experiments are designed:

- (i) Firstly, to verify the effectiveness of the function-fitting-based method of periodic disturbance compensation, the following four experimental preparations are made:
 1. Speed open loop control.
 2. Do not apply ASMADO.
 3. Use a hysteresis brake to provide constant resistance torque.

TABLE 2 Rated parameters of the PMSM.

Parameters	Values
Rated voltage [V]	24
Rated current [A]	0.75
Rated torque [N m]	0.8
Rated speed [rpm]	300
Number of pole pairs [-]	14
Weight [g]	247

TABLE 3 Parameters of ILC.

Parameters	Symbols	Values
Speed command [$^{\circ}$ /s]	ω_d	3
Proportional gain of ILC controller [-]	P	75
Integral gain of ILC controller [-]	I	1200
Iterations [-]	K	3
Sampling frequency [KHz]	f	1

TABLE 4 Parameters of BPNN.

Parameters	Values
Number of data in the input/output sample set	120 000
Number of layers in the network	5
The nodes number of input layer	1
The nodes number of hidden layers	[15,20,15]
The nodes number of output layer	1

4. Make the control quantity $u = 1500$.

Then, compare the output of the torque sensor before and after applying for periodic disturbance compensation \hat{d}_p .

- (ii) Next, the RADC method proposed in this paper is compared with the traditional PI+DOB control method in speed tracking performance.

It is worth noting that to ensure the fairness of the comparison experiments, the hardware conditions, driver schemes, and controller parameters of different experiments are consistent.

5.1 | Experimental parameters

Tables 2–5 give the complete parameters list of the motor, ILC, BPNN, PI+DOB, and PI+RADC.

After much BPNN training, the calculation amount and goodness of fit are comprehensively considered. As shown in Table 4, it was decided to set three hidden layers, each layer containing 15, 20, and 15 nodes, respectively. In addition, the strategy of early termination is adopted to prevent overfitting.

TABLE 5 Parameters of two control methods (PI+RADC and PI+DOB) and system.

Parameters	Symbols	Values
Equivalent nominal moment of inertia [-]	J_n	0.3
Equivalent nominal damping coefficient [-]	B_n	13
Speed command [$^{\circ}$ /s]	ω_d	1→1.3
Proportional gain of PI controller [-]	k_p	75
Integral gain of PI controller [-]	k_i	1200
The cutoff Angle frequency of DOB [rad/s]	g	100
Sliding mode surface parameter [-]	c	50
Adaptation law parameter 1 [-]	σ_1	0.1
Adaptation law parameter 2 [-]	σ_2	1
Sliding mode gain [-]	β	0.05
Boundary thickness [-]	ν	0.1
Preset switching gain [-]	Λ	0.1

5.2 | Experimental results

When training BPNN, this experiment randomly selects 80% of the datasets for training, 10% for verification and 10% for testing. Figure 6 shows the fitting effect of the disturbance function based on BPNN on real periodic determinable disturbance. From the experimental results, it can be seen that \hat{d}_p is equivalent to d_p in the complete period of motor periodic disturbance. And as shown in Figure 7, it is the linear regression graph for training BPNN. It describes the correlation among the training set, verification set, test set, and overall results after training. Where the abscissa represents the target output, the ordinate represents the fitting function between the predicted output and the target output, and R is the correlation coefficient. The closer the R value is to 1, the more intimate the relations between prediction and output data are. And the closer the R value is to 0, the more random the relationship between prediction and output data is. In this experiment, the correlation coefficient R can reach 0.983.

Figure 8 depicts the output of the torque sensor before and after applying for periodic disturbance compensation when the speed is open loop. When there is no disturbance compensation, the output of the torque sensor has obvious sudden changes. After the disturbance compensation based on BPNN is used to compensate for the periodic disturbance, the torque curve is improved, and the fluctuation is reduced.

Figure 9 depicts the speed tracking curves under the PI+DOB and PI+RADC methods when the speed command is a step command of 1 to 1.3 $^{\circ}$ /s. As can be seen from Figure 9, the speed fluctuation range under the PI+RADC method is relatively small during steady-state tracking, and the speed error can be controlled within 5% of the speed command. The PI+RADC method can achieve fast tracking during dynamic tracking with insignificant overshoot.

In addition, some statistical analysis was done on the speed error e during the first 20 s steady state, as shown in Table 6

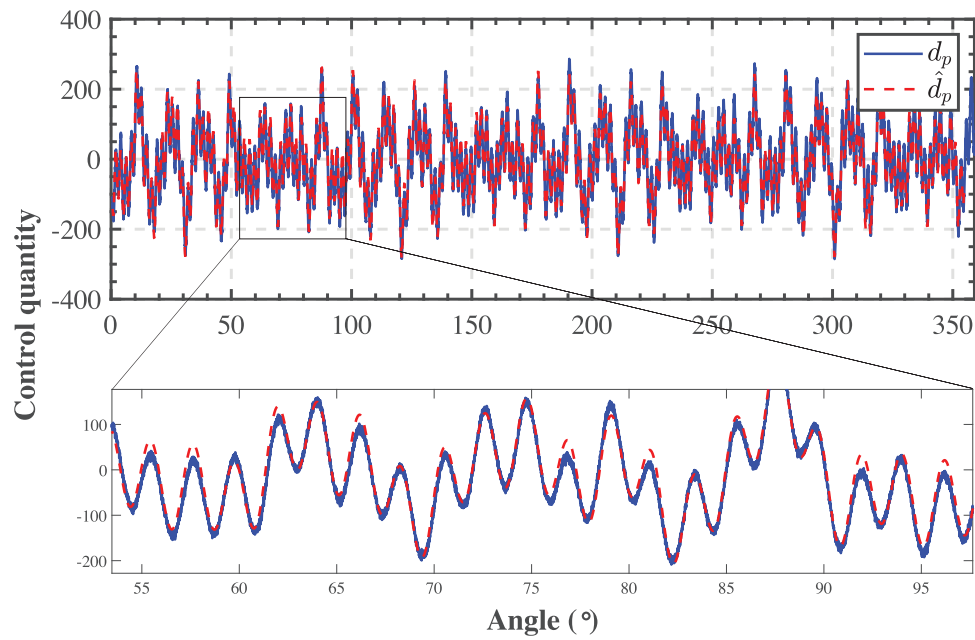


FIGURE 6 Fitting effect diagram of disturbance function based on BPNN for real periodic determinable disturbance.

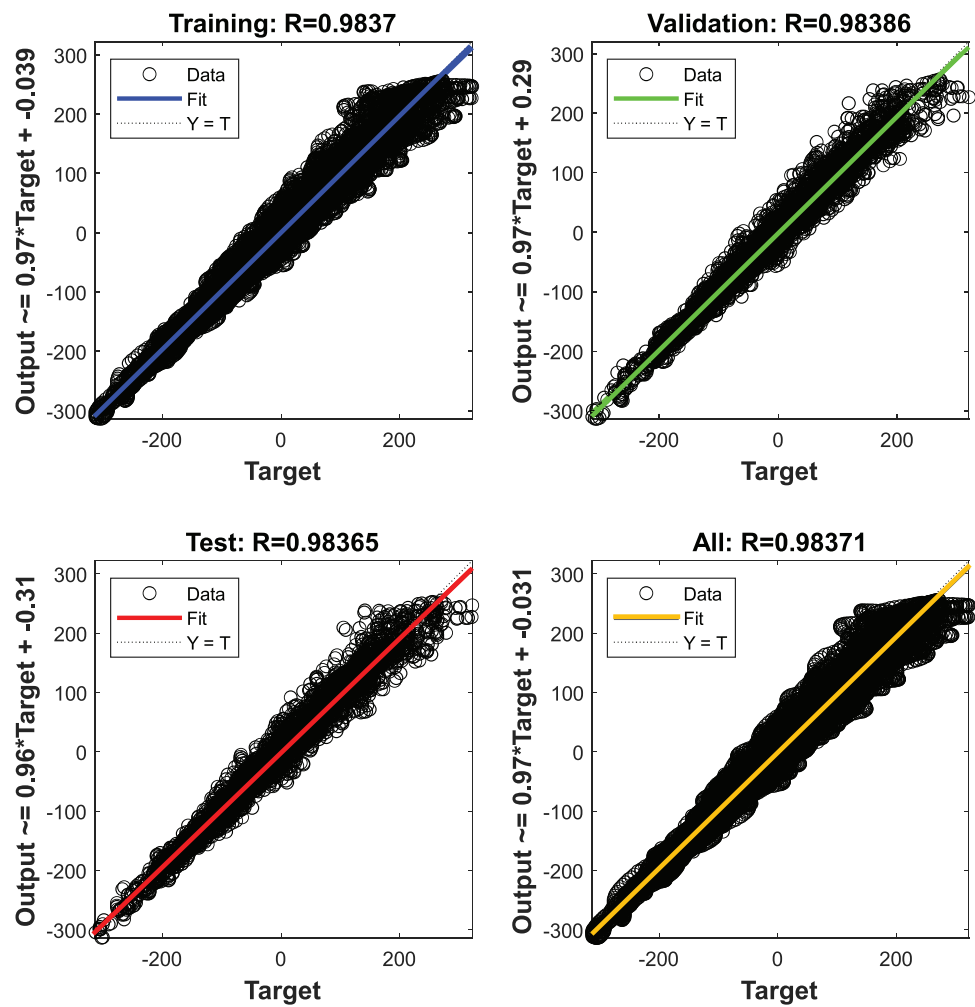


FIGURE 7 Linear regression graph of training BPNN.

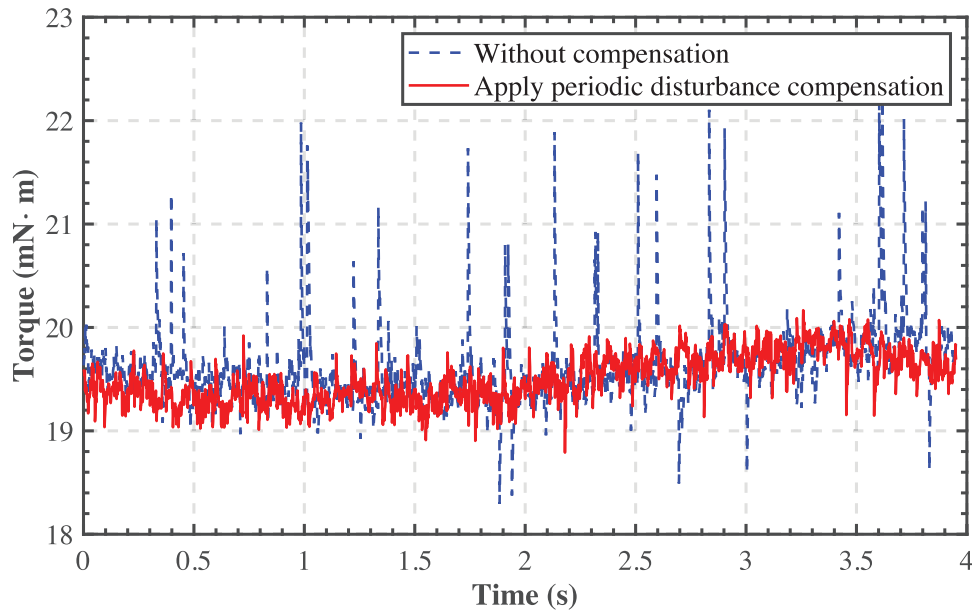


FIGURE 8 When the speed is open loop, the output of torque sensor before and after applying periodic disturbance compensation.

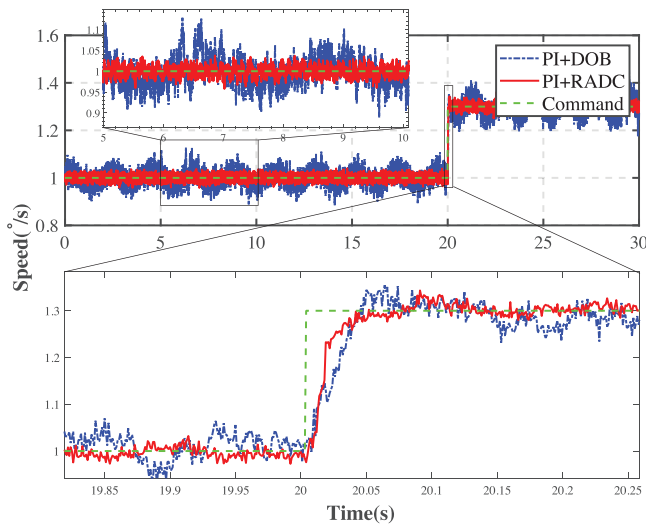


FIGURE 9 Speed tracking curves under different control methods.

and Figure 10. Table 6 lists the maximum (Max), mean and standard deviation (STD) of the speed error e for both control algorithms. In this case, all three performance indicators of PI+RADC are lower than PI+DOB. Moreover, the speed error can be controlled within $0.0425^\circ/\text{s}$. Figure 10 shows the his-

TABLE 6 Max, mean, and STD of speed error e ($e = \omega_d - \omega_m$).

	PI+DOB	PI+RADC
Max($ e $) [$^\circ/\text{s}$]	0.1282	0.0425
Mean(e) [$^\circ/\text{s}$]	$7.2503e^{-4}$	$8.0355e^{-5}$
STD(e) [$^\circ/\text{s}$]	0.0321	0.0113

togram of the distribution of e . The distribution histograms of both control methods show good normal distribution characteristics, but the distribution of PI+RADC is dense compared to PI+DOB.

The above results show that the RADC method is better at improving the immunity of a particular controlled object and reducing the speed fluctuations of the motor, reflecting the superiority of the proposed method.

6 | CONCLUSION

This paper focuses on the problem of disturbance suppression in low-speed PMSM servo systems when using the current-loop-free control method. A new active hierarchical refined anti-disturbance controller, the RADC, is proposed.

Complex multi-source disturbances are classified into the periodic determinable disturbance and the indeterminate residual disturbance according to their characteristics. BPNN based on ILC is used to fit the periodic disturbance. ILC aims to provide more comprehensive input and output datasets for BPNN training, rather than as the final controller. The RADC controller is used in the inner loop of the control, so that the BPNN-based offline disturbance compensator and ASMADO can compensate for the above two kinds of disturbances hierarchically. The offline disturbance compensator obtained by fitting the BPNN is a continuous function of the angular position of the motor and the periodic disturbance, allowing accurate and fast compensation of periodic disturbance at any position of the motor. The ASMADO consists of a DOB and an ASMC. First, the DOB is constructed to observe disturbances in the low-frequency domain. Then, the ASMC is then not used as a controller but is designed to assist the DOB in estimating

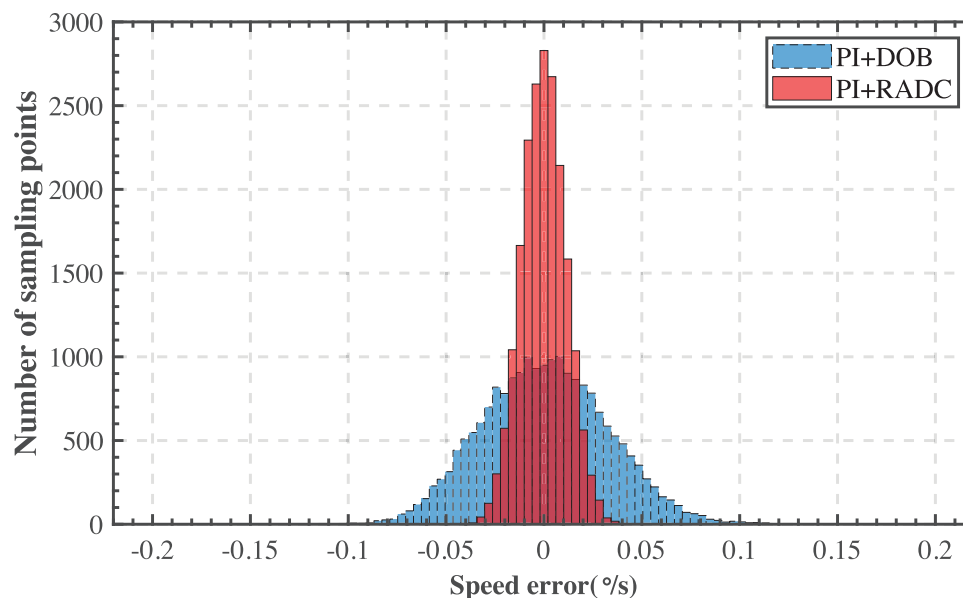


FIGURE 10 Speed error e distribution histogram under different control methods.

and compensating for high-frequency disturbances. Besides, the adaptive switching gain is automatically adjusted with the sliding mode state, which not only allows the system to converge quickly but also reduces the system jitter at a steady state with better robustness.

The experimental results demonstrate the effectiveness and superiority of the RADC. When the current-free-loop control method is used, the speed fluctuation of PMSM is still effectively suppressed, and the low-speed tracking performance is superior. Therefore, the proposed method is novel and necessary to improve the anti-disturbance performance of the PMSM in engineering applications.

AUTHOR CONTRIBUTIONS

Huifan Wang: Conceptualization, data curation, investigation, methodology, software, validation, visualization, writing-original draft, writing - review and editing. Junze Tong: Data curation, investigation, software, validation, visualization, writing - review and editing. Zhongshi Wang: Formal analysis, funding acquisition, project administration, resources, supervision, writing - review and editing. Dapeng Tian: Conceptualization, formal analysis, funding acquisition, project administration, resources, supervision, writing - review and editing.

ACKNOWLEDGMENTS

This research was supported by the National Natural Science Foundation of China [Grant no. T2122001] and [Grant no. 62203421], National Key R&D Program of China [Grant no. 2022YFF1302000] and Changchun Science and Technology Development Program [Grant no. 21SH03].

CONFLICT OF INTEREST

The authors declare no conflict of interest.

DATA AVAILABILITY STATEMENT

Research data are not shared.

ORCID

Huifan Wang  <https://orcid.org/0000-0002-9169-2932>

Junze Tong  <https://orcid.org/0009-0000-3770-5555>

Zhongshi Wang  <https://orcid.org/0000-0003-3674-2623>

Dapeng Tian  <https://orcid.org/0000-0002-3438-2970>

REFERENCES

- Gmati, B., Jlassi, I., Khojet.El.Khil, S., Marques.Cardoso, A.J.: Open-switch fault diagnosis in voltage source inverters of PMSM drives using predictive current errors and fuzzy logic approach. *IET Power Electron.* 14(6), 1059–1072 (2021)
- Shi, T., Wang, Z., Xia, C.: Speed measurement error suppression for PMSM control system using self-adaption Kalman observer. *IEEE Trans. Ind. Electron.* 62(5), 2753–2763 (2014)
- Junejo, A.K., Xu, W., Mu, C., Liu, Y.: Improved continuous fast terminal sliding mode control for speed regulation of surface-mounted permanent magnet synchronous motor. In: 2018 21st International Conference on Electrical Machines and Systems (ICEMS), pp. 93–98. IEEE, Piscataway, NJ (2018)
- Abbaszadeh, K., Alam, F.R., Saied, S.: Cogging torque optimization in surface-mounted permanent-magnet motors by using design of experiment. *Energy Convers. Manage.* 52(10), 3075–3082 (2011)
- Wang, Y., Gao, Y., Zhao, C., Li, X.: Iterative learning based torque ripple suppression of flux-modulation double-stator machine. *IEEE Trans. Ind. Electron.* 69(7), 6645–6656 (2021)
- Yu, J., Shi, P., Dong, W., Chen, B., Lin, C.: Neural network-based adaptive dynamic surface control for permanent magnet synchronous motors. *IEEE Trans. Neural Networks Learn. Syst.* 26(3), 640–645 (2014)
- Ma, Y., Li, D., Li, Y., Yang, L.: A novel discrete compound integral terminal sliding mode control with disturbance compensation for PMSM speed system. *IEEE/ASME Trans. Mechatron.* 27(1), 549–560 (2021)
- Bien, Z., Xu, J.X.: *Iterative Learning Control: Analysis, Design, Integration and Applications.* Springer, Berlin, Heidelberg (2012)
- Sebastian, G., Tan, Y., Oetomo, D.: Convergence analysis of feedback-based iterative learning control with input saturation. *Automatica* 101, 44–52 (2019)

10. Fei, Q., Deng, Y., Li, H., Liu, J., Shao, M.: Speed ripple minimization of permanent magnet synchronous motor based on model predictive and iterative learning controls. *IEEE Access* 7, 31791–31800 (2019)
11. Liu, J., Li, H., Deng, Y.: Torque ripple minimization of PMSM based on robust ILC via adaptive sliding mode control. *IEEE Trans. Power Electron.* 33(4), 3655–3671 (2017)
12. Jiang, J., Chen, Z., Wang, Y., Peng, T., Zhu, S., Shi, L.: Parameter estimation for PMSM based on a back propagation neural network optimized by chaotic artificial fish swarm algorithm. *Int. J. Comput. Commun. Control* 14(6), 615–632 (2020)
13. Utkin, V., Guldner, J., Shi, J.: *Sliding Mode Control in Electro-mechanical Systems*. CRC Press, Boca Raton, FL (2017)
14. Zhao, Y., Liu, X.: Speed control for PMSM based on sliding mode control with a nonlinear disturbance observer. In: 2019 Chinese Automation Congress (CAC), pp. 634–639. IEEE, Piscataway, NJ (2019)
15. Guo, X., Bai, D., Zhou, S., Fan, T.: A PMSM sliding mode control system based on a novel exponential reaching law. *Control Eng. China* 25(10), 1865–1870 (2018)
16. Lu, H., Yang, D., Su, Z.: Improved sliding mode control for permanent magnet synchronous motor servo system. *IET Power Electron.* (2022)
17. Liu, J., Li, H., Deng, Y.: Current adaptive sliding mode control based on disturbance observer for permanent magnet synchronous motor. *Opt. Precis. Eng.* 25(5), 1229–1241 (2017)
18. Guo, L., Feng, C.B., Chen, W.H.: A survey of disturbance-observer-based control for dynamic nonlinear system. *Dyn. Contin. Discrete Impulsive Syst., Ser. B: Appl. Algorithms* 13, 79–84 (2006)
19. Guo, L., Chen, W.H.: Disturbance attenuation and rejection for systems with nonlinearity via DOBC approach. *Int. J. Robust Nonlinear Control* 15(3), 109–125 (2005)
20. Guo, L., Cao, S.: Anti-disturbance control theory for systems with multiple disturbances: a survey. *ISA Trans.* 53(4), 846–849 (2014)
21. Tian, D., Yashiro, D., Ohnishi, K.: Improving transparency of bilateral control system by sliding mode assist disturbance observer. *IEEE Trans. Electr. Electron. Eng.* 8(3), 277–283 (2013)
22. Tian, D., Zhang, Y.: Remote haptic sensing using sliding-mode assist disturbance observer as force detector. *IET Control Theory Appl.* 9(10), 1517–1524 (2015)
23. Dosiek, L., Pillay, P.: Cogging torque reduction in permanent magnet machines. *IEEE Trans. Ind. Appl.* 43(6), 1565–1571 (2007)
24. Husev, O., Roncero-Clemente, C., Makovenko, E., Pimentel, S.P., Vinnikov, D., Martins, J.: Optimization and implementation of the proportional-resonant controller for grid-connected inverter with significant computation delay. *IEEE Trans. Ind. Electron.* 67(2), 1201–1211 (2019)
25. Wang, R., Xu, H., Li, B., Feng, Y.: Research on method of determining hidden layer nodes in BP neural network. *Comput. Technol. Dev.* 28(4), 31–35 (2018)
26. Zhu, Y., Qiao, J., Guo, L.: Adaptive sliding mode disturbance observer-based composite control with prescribed performance of space manipulators for target capturing. *IEEE Trans. Ind. Electron.* 66(3), 1973–1983 (2018)
27. Moulay, E., Perruquetti, W.: Finite time stability and stabilization of a class of continuous systems. *J. Math. Anal. Appl.* 323(2), 1430–1443 (2006)
28. Zhu, Z., Xia, Y., Fu, M.: Attitude stabilization of rigid spacecraft with finite-time convergence. *Int. J. Robust Nonlinear Control* 21(6), 686–702 (2011)
29. Hu, Q., Li, B., Qi, J.: Disturbance observer based finite-time attitude control for rigid spacecraft under input saturation. *Aerosp. Sci. Technol.* 39, 13–21 (2014)

How to cite this article: Wang, H., Tong, J., Wang, Z., Tian, D.: ASMADO-based refined anti-disturbance low-speed control of PMSM. *IET Power Electron.* 16, 1605–1619 (2023). <https://doi.org/10.1049/pel2.12501>